



Enhancing fruit disease classification with an advanced 3D shallow deep neural network for precise and efficient identification

Hridaynath Pandurang Khandagale^{a,b,*}, Sangram Tukaram Patil^c, Vikram Sampat Gavali^d, Amrita Arvind Manjrekar^e, Pratap Pandurang Halkarnikar^f

^a Research Scholar, Computer Science and Engineering, D Y Patil Agriculture and Technical University, Talsande, Kolhapur, Maharashtra, India

^b Department of Technology, Shivaji University, Kolhapur, Maharashtra, India

^c School of Engineering & Technology, D Y Patil Agriculture & Technical University, Warana – Wathar Road, Talsande Fata, Talsande, Kolhapur, India

^d Department of Artificial Intelligence & Machine Learning, New Institute of Technology, Kolhapur, Maharashtra, India

^e Computer Science and Technology, Department of Technology, Shivaji University, Kolhapur, Maharashtra, India

^f Dept of Computer Engineering, Dr. D.Y.Patil Institute of Engineering, Management & Research, Akurdi, Pune, India

ARTICLE INFO

Keywords:

Crisscross Harris Hawks Optimizer
Fruit disease
Newton Time-Extracting Wavelet Transform
Regularized Bias-Aware Ensemble Kalman Filtering
3D Shallow Deep Neural Network

ABSTRACT

Diseases in fruits cause major problems in the agricultural industry and lead to significant economic loss. These diseases reduce yields, degrade the variety and can lead to crops being withdrawn from cultivation. Existing methods rely on heavy-weight architectures, which require higher storage capacity and expensive training operations due to the large number of parameters involved. In this paper, Enhancing Fruit Disease Classification with an Advanced 3D Shallow Deep Neural Network for Precise and Efficient Identification (EFDDNN-EI) is proposed. Here, the input images are taken from two datasets: (i) Strawberry Diseases dataset, (ii) Apple Fruit Disease dataset. The input images from both datasets are pre-processed by Regularized Bias-Aware Ensemble Kalman Filtering (RBAEKF) to eliminate unwanted noise. The pre-processed images are fed to the Newton Time-Extracting Wavelet Transform (NTEWT) to extract relevant attributes, such as color, texture, shape, size. The extracted features are fed into the 3D Shallow Deep Neural Network (3DSDNN). The 3DSDNN classifies the input images from the Strawberry Diseases dataset as botrytis cinerea, slugs, aphids, sunburn, thrips, root rot, vegetable green insects, viral diseases, powdery mildew and healthy leaves. Similarly, images from the Apple Fruit Disease dataset are classified into categories, like Blotch Apple, Normal Apple, Rot Apple, Scab Apple. Finally, Crisscross Harris Hawks Optimizer (CCHHO) is employed to enhance EFDDNN-EI that can classify the fruit diseases by maximizing the accuracy and minimizing the computation time. The proposed EFDDNN-EI approach is implemented, and the performance metrics, like recall, f1-score, precision, testing accuracy, testing loss and ROC to assess the efficacy of the method. The EFDDNN-EI technique achieves 16.89%, 18.57% and 27.68% higher testing accuracy, and 18.81%, 26.53% and 30.62% higher recall compared to the existing approaches: Strawberry Disease Detection under Transfer Learning of Deep Convolutional Neural Networks (SDD-TLDCNN), A Better, Lightweight YOLOV5 Algorithm for Strawberry Disease Identification (SDD-YOLOV5), and Structural Invariant Feature Segmentation dependent Apple Fruit Disease Detection utilizing Deep Spectral Generative Adversarial Networks (SIFFD-DSGAN).

1. Introduction

Fruit diseases pose a constant threat to farmers and cause significant economic losses. Anthracnose is an example of a fruit disease that, if left unnoticed, can lead to severe fruit rot infections (Haq et al., 2024). In this regard, precision agriculture offers a number of technologies to support

farmers' decision-making (Wu et al., 2024). Strawberry is an edible fruit for eating, and it has high nutritional content and economic value. Numerous bacteria, viruses and phytopathogenic fungi can easily infect strawberries (Fischer-Brandies et al., 2025). Colletotrichum siamense, the anthracnose-causing organism and the Graymold is caused by Botrytis cinerea (Annapoorna, 2024; Balu, Ganapathy, Arya, Atchudan,

* Corresponding author.

E-mail addresses: hpk_tech@unishivaji.ac.in (H.P. Khandagale), sangrampatil@dyp-atu.org (S.T. Patil), vikram25g@gmail.com (V.S. Gavali), aam_tech@unishivaji.ac.in (A.A. Manjrekar), pp.halkarnikar@dypiemr.ac.in (P.P. Halkarnikar).

& Sundramoorthy, 2024; Selvaraj, Venkatesan, Ganapathy, & Sathish-kumar, 2024). The primary pathogens that damage strawberries are Neopestalotiopsis spp (Gupta et al., 2025), which causes fruit rot, crown rot, blade blight and other fungal diseases that result in powdery mildew, a disease that mostly attacks the leaves, fruits and petioles (Liu et al., 2025). These diseases have a detrimental effect on fruit quality, growth and productivity by interfering with photosynthesis (Oliullah et al., 2025). Farmers manually diagnose strawberry diseases, which takes more time and effort. This issue is further complicated by the declining workforce in agricultural areas, as it is very difficult to assess the severity of the disease on a large scale (Crespo et al., 2025). It is necessary to create an automated method that can quickly and accurately identify the fruit diseases. Nowadays, Artificial Intelligence (AI) has been utilized to diagnose agricultural illnesses with deep learning skills (Guo et al., 2025). Crop disease detection has found very accurate and cost-effective technique picture identification (Azizi et al., 2024; Ahmed and Yadav, 2024). Agriculture also makes extensive use of computer technologies (Gupta and Tripathi, 2024). It introduced a method for segmenting strawberries using deep learning algorithms (Hu et al., 2024). The scientists used a new dataset of 3100 images to train (Mehta et al., 2024; Jeong et al., 2024). Many AI methods have been put out to estimate the quality of strawberries. Since strawberries are high in nutritional value, they are recognized as a notable fruit for their wonder-full and delicious features, and they play an important role of agricultural sector (Jeong et al., 2024; Nguyen et al., 2024; Upadhyay and Gupta, 2024; Iqbal et al., 2025; Wang et al., 2024; Shafik et al., 2024; Raza et al., 2024).

Numerous bacterial, viral and fungal illnesses can harm strawberries, and each has unique symptoms. However, many diseases can present with similar symptoms, making an accurate diagnosis difficult. In addition, the detection of diseases might be made more difficult by external circumstances and other stressors. Thus, the key to managing strawberry diseases efficiently is the development of robust and efficient detection technologies, such as molecular diagnostic tools or enhanced imaging techniques.

The novelty of this work is the combination of multiple methods to improve the classification of fruit diseases with particular emphasis on strawberry and apple diseases. Through the application of a mixture of RBAEKF for image denoising and NTEWT for feature extraction, this method guarantees high-quality input images. The following categorization of strawberry and apple fruit disease using 3DSDNN is even further enhanced by the development of the CCHHO that not only enhances accuracy but also decreases the processing time. The proposed method corrects the deficiencies of existing models by adopting a fast optimization mechanism, thus enabling improved fruit disease classification with less processing period.

The key contributions of this paper are:

- Enhancing Fruit Disease Classification with an Advanced 3D Shallow Deep Neural Network for Precise and Efficient Identification (EFDDNN-EI) is proposed.
- This work introduces a novel pre-processing technique using RBAEKF to effectively remove noise from input images, ensuring clearer data for classification.
- The NTEWT is applied to extract essential attributes like color, texture, shape and size from fruit disease images, enhancing feature representation.
- The 3DSDNN is employed for accurate classification of diseases in both strawberry and apple datasets, improving recognition of various disease types.
- The CCHHO is integrated into the system, optimizing the deep learning model's parameters to boost classification precision and reduce computation time effectively.
- This work addresses existing limitations in disease classification models by combining advanced techniques, improving accuracy and efficiency while offering practical solutions in agriculture.

Continuing paper is designed as: **Section 2** divulges literature review; **Section 3** designates the proposed methodology; **Section 4** provides the results and discussion; **Section 5** presents conclusion.

2. Literature survey

Numerous studies have been submitted previously in the literature on fruit diseases classification, few of them are reviewed here,

Karki et al., (2024) presented a transfer learning method in deep convolutional neural networks (CNNs) for detecting some strawberry ailments. Using fine-tuning as well as feature extraction of transfer learning and compared devoid of transfer learning. Angular leaf spot, anthracnose, grey mold, powdery mildew were some of the target illnesses for identification on fruit and leaves. It has higher testing accuracy and lower recall.

Chen et al., (2023) presented an enhanced lightweight Yolov5 system for recognizing strawberry ailments. The backbone network integrates a convolutional block attention module (CBAM) for enhance its capacity to extract characteristics linked to strawberry illness and inhibit extraneous input. It has high recall and high computation time.

Subha and Kasturi, (2024) introduced the Deep Spectral Generative Adversarial Networks (DSGANs) approach for apple disease categorization. Self-Adaptive Plateau Histogram Equalization (SAPHE) optimized segmentation and Modified Gabor kernels were used for feature extraction. DSGANs were employed for classification, iteratively refining feature margins for accurate disease detection. It has high specificity and less accuracy.

Paliwal et al., (2024) introduced an automatic apple classification depending on the concept of deep learning. The training process train the neural network using the CNN, and then it test the model with a random image given by the user. The system was able to classify the image as a rotten fruit or a fresh fruit based on different apple fruit diseases. It has high recall and low precision.

Zhang et al., (2023) introduced the gray mold and anthracnose disease hyper spectral imaging for strawberry leaf detection. The Support Vector Machine (SVM) was applied for the initial finding of strawberry graymold and anthracnose through spectrum fingerprints, VIS, and its consolidated features as components. It has higher recall and higher computation time.

Wu et al., (2023) presented the early identification of strawberry leaves illness using hyper spectral imaging combining textural, multiple vegetation indices and spectral features. The effective TFS was chosen using correlation-based selecting features, the OWS was selected using Competing Adaptive Reweighted Sampling (CARS). It has lower computation time and lower recall.

Acharya and Ravi, (2024) presented Capsule Neural Network (Cap-sNet) structure along modified the network structure through including additional convolution layers to improve the learning capability of the method to categorize the apple infections as apple rust, apple scab, healthy as well as multi diseases on the same leaf. Experimentation was performed on Kaggle Plant Pathology 2020 – FGVC7 database. It has higher specificity and lesser accuracy.

Table 1 reviews advances in strawberry and apple disease detection using deep learning and hyperspectral imaging. Despite high accuracy, issues like low recall, slow inference, poor generalization and limited datasets persist. Emerging models and multi-modal approaches show promise but require improvements for real-time, robust and scalable agricultural disease diagnosis.

3. Proposed method

This segment deliberates the proposed EFDDNN-EI approach. The aim is to develop an early, accurate and non-destructive disease identification system for strawberry and apple plants by integrating hyperspectral imaging with deep learning techniques. This system can use spectral and vegetation features to enhance diagnostic accuracy and

Table 1
Literature Survey.

Authors and reference	Methods	Advantages	Disadvantages
Karki et al., (2024)	Transfer Learning (CNNs: VGG19, Inception V3, ResNet50, DenseNet121)	High accuracy	Low recall
Chen et al., (2023)	Enhanced Lightweight Yolov5 with GhostConv and CBAM	High recall	High computation time
Subha and Kasturi, (2024)	Deep Spectral Generative Adversarial Networks	High specificity	Low accuracy
Paliwal, (2024)	Deep Learning, Convolutional Neural Network	High accuracy	Low precision
Zhang et al., (2023)	support vector machine (SVM)	High recall	High computation time
Wu et al., (2023)	support vector machine (SVM), K-nearest Neighbor (KNN)	Low computation time	Low recall
Acharya and Ravi, (2024)	Capsule Neural Network (CapsNet)	High specificity	Low accuracy

facilitate real-time disease monitoring in agricultural settings.

Fig. 1 shows the EFDDNN-EI block diagram. The method combines hyperspectral imaging with deep learning for early fruit disease detection. It captures hyperspectral images, extracts spectral and vegetation features, applies feature selection, and trains models like CNN, LSTM and Capsule Networks enabling accurate, real-time and non-destructive diagnosis for precision agriculture.

3.1. Data Acquisition

The input images are gathered through Strawberry Disease (<https://universe.roboflow.com/research-proj/strawberry-diseases-detection/dataset/1>) and Apple Fruit Disease (<https://www.kaggle.com/datasets/anilsandhii/apple-fruit-disease-images-dataset>) datasets and these dataset descriptions are given below.

3.1.1. Strawberry disease dataset

This dataset is obtained from Roboflow's research project repository. It contains annotated images of strawberry leaves affected by various diseases, such as leaf scorch and powdery mildew. The dataset includes 11,795 images and is organized into different disease categories. The dataset was partitioned into 70 % (10,317 imageries) for training, 15 % (992 imageries) for validation and 15 % (486 imageries) for testing.

3.1.2. Apple fruit disease dataset

This dataset is obtained from Kaggle and has high-quality imageries of apple fruits suffered by different infections, like Apple Scab, Black Rot, Cedar Apple Rust. This dataset comprises over 3,971 labeled images categorized by disease type. The dataset is separated as three subsets: 70 % (2,779 imageries) for training, 15 % (595 imageries) for testing and 15 % (597 imageries) for validation.

3.2. Pre-processing under RBAEKF

The pre-processing utilizing RBAEKF (Nóvoa et al., 2024) is described here. The RBAEKF is applied for enhance the input image and eliminate noise. The dynamic model of a system and its known control inputs are used in Kalman filtering. RBAEKF enhances the precision of system state variable estimation by merging the advantages of ensemble Kalman filtering and bias correction. Because RBAEKF accounts for model and observation biases, it produces estimates that are more reliable than traditional data assimilation methods. The RBAEKF requires a

bias and gradient model using equation (1).

$$\tau(\psi_j) = \|\psi_j - \psi_j^f\|_{c_{\psi\psi}^{-1}}^2 + \|y_j - d_j\|_{c_{dd}^{-1}}^2 + \gamma \|b_j\|_{c_{bb}^{-1}}^2 \quad (1)$$

where τ represents the images embedded in the off j at layer $f-1$; $\psi_j - \psi_j^f$ represents the image initialization, which are collected from the strawberry dataset; $\gamma \|b_j\|_{c_{bb}^{-1}}^2$ denotes the size of image pixel; $\|y_j - d_j\|_{c_{dd}^{-1}}^2$ denotes the c_{dd}^{-1} number of images from the noise affected images; $\|\psi_j - \psi_j^f\|_{c_{\psi\psi}^{-1}}^2$ epitomizes the normalized of noise free images and d implies coefficient that lessen the model's sensitivity of image pixels. The broad RBAEKF of this concept raises the issue of noise contamination once, when filtering content-level preferences, noise compressed to both healthy and diseased images and it is given in equation (2).

$$\frac{1}{2} \frac{d\tau}{d\psi} \Big|_{\psi_j^a} = c_{\psi\psi}^{f-1} (\psi_j^a - \psi_j^f) + \frac{dy_j}{d\psi_j} \Big|_{\psi_j^a}^T c_{dd}^{-1} (y_j^a - d_j) + \gamma \frac{db_j}{d\psi_j} \Big|_{\psi_j^a}^T c_{bb}^{-1} b_j^a = 0 \quad (2)$$

where $\frac{dy_j}{d\psi_j}$ denotes the aggregation of neighbour pixel over the user-item-entity image; $\gamma \|b_j\|_{c_{bb}^{-1}}^2$ represents the c_{bb}^{-1} number of images from the noise affected images; $(\psi_j^a - \psi_j^f)$ represents the normalized of noise free images; d refers coefficient that decrease the model's sensitivity of image pixels; c_{dd}^{-1} signifies size of image pixel and $c_{\psi\psi}^{-1}$ signifies the multimodal image preferences with high-order semantic noise level. To model preferences at the semantic noise level, the processed semantic images from the dataset images of various noises and add them to the bipartite user-item graph which is given in equation (3).

$$b_j^a \approx b_j^f + J^f M (\psi_j^a - \psi_j^f) \quad (3)$$

here b_j^a refers length of original and neighbour pixel in noise dimension; b_j^f signifies image are scaled or resize; ψ_j^a and ψ_j^f specifies neighbours of c_{bb}^{-1} pixel for both healthy and diseased images; d states coefficient that decrease the model's sensitivity of image pixels; J^f embodies c_{bb}^{-1} number of images from the noise affected images; f signifies size of image pixel; M represents the noises in textual images and $(\psi_j^a - \psi_j^f)$ indicates the total number of processed images. Therefore reducing noise pollution and enhancing the use of multimodal information using equation (4).

$$\psi_j^a = \psi_j^f + K \left[\left(\prod + J^f \right) MC_{\psi\psi}^f M^T \left(\prod + J^f \right)^T + \gamma C_{dd} C_{bb}^{-1} J^f M C_{\psi\psi}^f M^T J^f \right]^{-1} \quad (4)$$

where ψ_j^a denotes the neighbour pixel of entity image from strawberry dataset; d represents coefficient that lessen the model's sensitivity of image pixels; $(\prod + J^f)$ symbolizes the C_{bb}^{-1} number of images from the noise affected images; $MC_{\psi\psi}^f$ indicates the complete quantity of images that have been processed and M^T denotes the noises in textual images and pixel modes. The noise is eliminated using equation (5).

$$K = C_{\psi\psi}^f M^T \left[C_{dd} + \left(\prod + J^f \right) MC_{\psi\psi}^f M^T \left(\prod + J^f \right)^T + \gamma C_{dd} C_{bb}^{-1} J^f M C_{\psi\psi}^f M^T J^f \right]^{-1} \quad (5)$$

consider K as hyper-parameter that adjusts total modality contributes to noise eliminated image pixels; d as coefficient that reduce the model's sensitivity of image pixels; $C_{\psi\psi}^f$ signifies the C_{bb}^{-1} number of images from the noise affected images; $(\prod + J^f)$ indicates the size of image pixel; M^T means the interacted image set, $MC_{\psi\psi}^f$ means total processed images.

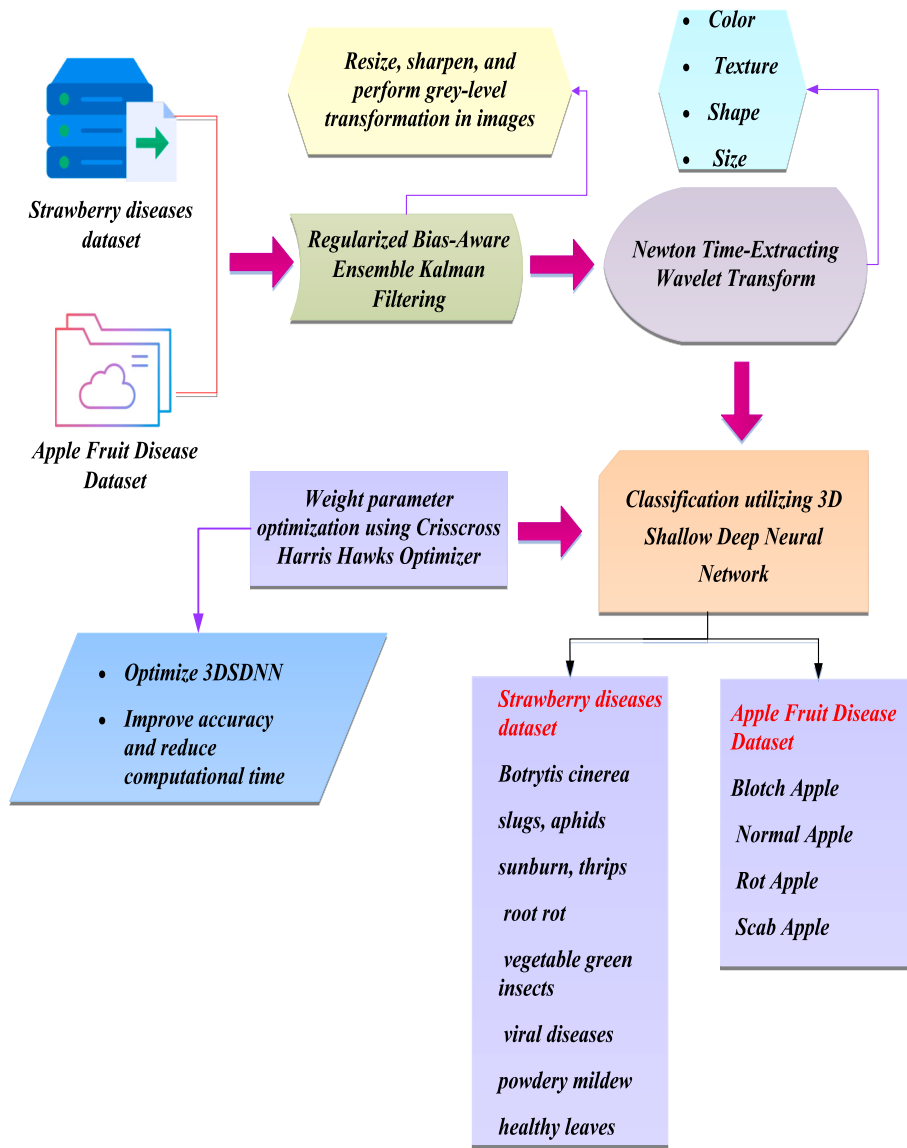


Fig. 1. Block diagram for EFDDNN-EI approach.

Finally, the RBAEKF remove the noises from both the input and processed pictures then given to the feature extraction stage.

3.3. Feature extraction using Newton Time-Extracting wavelet transform

The feature extraction under NTEWT (Li et al., 2023) is explained here. NTEWT is used to extracting the specified characteristics from images, like colour, texture, shape and size. To enhance its ability to process nonstationary images, the approach incorporates NTEWT instantaneous image estimation and extends the synchroextracting transform to the wavelet transform. The proposed approach maintains strong invertibility while offering concentrated representation at various resolutions. NTEWT extracts features accordingly from the pre-processed imageries. The main objective of the NTEWT is to use ridge curve identification to develop a new extraction operator. This is expressed in equation (6).

$$NTe(b, a) = W_X^{\psi}(b, a) \cdot \delta(b - \bar{t}_X(b, a)) \quad (6)$$

here NTe designates with regard to wavelet functions; (b, a) represent the chirp rate estimator and extracting the strawberry disease; W_X^{ψ} implicates time duration of every once iteration, δ means pixel reduction in

images. The reversibility is retained by the NTEWT that just reassigns the wavelet coefficients in the image direction using equation (7).

$$X\left(\frac{\omega_y}{a}\right) = \frac{aW_X^{\psi}\left(\alpha'\left(\frac{\omega_y}{a}\right), a\right)e^{-i\frac{\omega_y}{a}b}}{C_X\left(\alpha'\left(\frac{\omega_y}{a}\right), a\right)} \quad (7)$$

where $\left(\frac{\omega_y}{a}\right)$ as chirp rate estimator and extracting the strawberry disease; X as time duration of every once iteration; W_X^{ψ} as neighbour-hood pixel and $\left(\frac{\omega_y}{a}\right)$ as second order neglecting in images. It extracting each strawberry image according to pixels duration has good mustier solution using equation (8).

$$X\left(\frac{\omega_y}{a}\right) = \frac{aNTe\left(\alpha'\left(\frac{\omega_y}{a}\right), a\right)e^{-i\frac{\omega_y}{a}b}}{C_X\left(\alpha'\left(\frac{\omega_y}{a}, a\right)\right)} \quad (8)$$

In this, $\left(\frac{\omega_y}{a}\right)$ refers chirp rate estimator and extracting the strawberry diseases; NTe symbolizes respect to wavelet functions; $\alpha'\left(\frac{\omega_y}{a}\right)$ as a reli-

able approximation of the instant extraction in images; $e^{-\frac{\omega_a}{a}b}$ denotes the total number of extracted images; C_x designates the parameter of the function and a denotes the pixel size. NTEWT is an image shape extraction technique. It incorporates concepts from Newton's root finding technique as well as wavelet transforms and it is given in equation (9).

$$\alpha(t) = \alpha(t) + \frac{\sum_{i=1}^N W_x(a_i, b_i) W_r^*(a_i, b_i)}{\sum_{i=1}^N |W_x(a_i, b_i)|^2} \quad (9)$$

in which (a_i, b_i) are the scale and translation parameters; $W_r^*(a_i, b_i)$ denotes the complex conjugate of $W_r(a_i, b_i)$ and an initial guess for the shape to be extracted is typically represented as $\alpha(t)$. In image processing, NTEWT is a size extraction approach. Using NTEWT, the size extraction is labelled in equation (10).

$$W_x(a, b) = \int_{-\infty}^{\infty} x(t) u_{a,b}^*(t) dt \quad (10)$$

here $u_{a,b}^*(t)$ designates the scaled-down and translated wavelet analysis; $x(t)$ symbolizes the image's wavelet transform; $u(t)$ denotes the analysing wavelet and (a, b) are the criteria for scale and translation. Finally, the NTEWT has extracted these features such as colour, texture, shape and size and authenticated the signature. These extracted features are given to 3DSDNN as an input to verify features from the strawberry plant image.

3.4. Fruit diseases detection using 3D Shallow Deep Neural Network

In this section, strawberry diseases detection using 3DSDNN (Kausar et al., 2023) is discussed for classifying the input images from the Strawberry Diseases dataset into categories such as botrytis cinerea, slugs, aphids, sunburn, thrips, root rot, vegetable green insects, viral diseases, powdery mildew and healthy leaves. The images from the Apple Fruit Disease dataset are classified as blotch, normal, rot and scab apple.

Fig. 2 depicts the architecture diagram of 3DSDNN. Each convolutional layer's constant input is added to its output to create a residual connection, pursued by sample normalisation with pooling to create the first output that is downsampled. When the convolutional layer is applied five times without downsampling, the output size remains the same even though the inputs are downsampled four times in the same

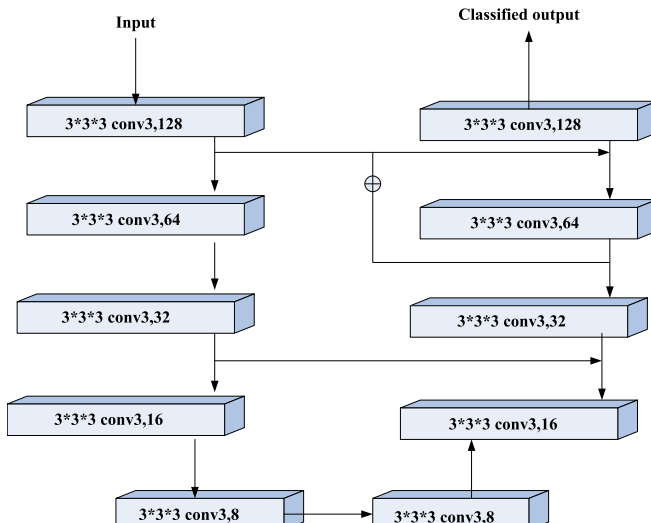


Fig. 2. Architecture diagram of 3DSDNN.

way. After that, upward convolutions follow the same tendency of adding skip connections and spatial information from the same down-sampling level. By using identity shortcuts at each stage, the network considers high- and low-level features extraction. Activation functions such as Leaky ReLU are used in every convolutional layer, while Softmax activation function concludes the final layer to attain final classification. To classify the fruit diseases, the 3DSDNN and an attention mechanism are added to the normal recurrent layer. 3DSDNN have been used extensively in many different disciplines due to their high feature extraction capabilities. Network layers are included in the heterogeneous model is exhibited in equation (11).

$$pDice_l(L_l'', R_l) = \overline{\left(\frac{\min(L_l'', 0.9) \cdot R_l}{\|R_l\|_2 + \|\min(L_l'', 0.9)\|_2} \right)} \quad (11)$$

where $pDice_l$ specifies image displays in the 3DSDNN neural layer's output in diverse scales; (L_l'', R_l) epitomizes line with images while kernels function; $\min(L_l'', 0.9)$ is the 3DSDNN activation function; R_l is the image operation in 3DSDNN; l signifies overall amount of layers' image scales; L_l'' signifies the images in the concealed layer's output and p indicates the order of supplied images time sequence. The incredibly complex nonlinear mapping connection of the actual sequence causes a noteworthy error accumulation effect, which has a negative impact on the categorization accurateness of strawberry disease prediction. using the equation (12).

$$loss(L_l'', i) = \sum_{vw} \frac{w^{-2}}{40} - \frac{1}{8} \sum_{l=1}^8 d(pDice(L_l'', R_l), i) \quad (12)$$

let $loss(L_l'', i)$ as activation image function value $\sum_{vw} \frac{w^{-2}}{40}; w$ as image displays in the 3DSDNN neural layer's output in diverse scales; L_l'' as 3DSDNN activation function; l represents total number of image scales in layer and R_l denotes the time sequence of the input images. The extracted features are supplied into 3DSDNN in various scales after the heterogeneous bi-directional layers are projected to categorize the original sequence in advance a pure DNN network is incapable to fully capture the information under equation (13).

$$d(l, i) = l + 100h(l, i) + 10h(l, i) \quad (13)$$

were d represents the heterogeneous bi-directional DNN layer's output when the image input is diverse, i implicates DNN image block in the heterogeneous bidirectional, $100h(l, i)$ denotes the tanh image activation function, l epitomizes total image scales in layer and $10h(l, i)$ designates the image displays in 3DSDNN neural layer's output in different scales. N which, 3DSDNN is fabricated to fully extract hidden information and the gate attention mode is connected to the Soft Max function to find aphids, slugs, sunburn, thrips, botrytis cinerea, green insects, powdery mildew and virus diseases in vegetables and it is given in equation (14).

$$h(l, i, v, t) = \text{sigmoid}(6(i-t)/t) (\max(v - l/v)^4) \quad (14)$$

here h denotes regression layer, l implies final diseases predictive strawberry; v exhibits the real value of diseases affected strawberry, i denotes the diseases prediction sequence's duration and t stands for the i^{th} pooling size of images. Finally, the 3DSDNN has classified the strawberry diseases as botrytis cinerea, slugs, aphids, sunburn, thrips, root rot, vegetable green insects, viral diseases, powdery milde and healthy leaves. Likewise, apple diseases are categorized as blotch, normal, rot and scab. The 3DSDNN classifier combines an AI-dependent optimization method because of its realism and importance. Here, CCHHO optimize the 3DSDNN, also 3DSDNN's weight and bias parameters are adjusted using CCHHO.

3.5. Optimization using Crisscross Harris Hawks Optimizer

The Crisscross Harris Hawks Optimizer (CCHHO) (Wang et al., 2023) is applied to increase the weight parameters h and d of 3DSDNN. The parameter h and d is enhanced to improve the accuracy and reduce the computation time. Fig. 3 portrays the flowchart of CCHHO for optimizing 3DSDNN parameter.

The CCHHO algorithm is inspired by the Harris's Hawks' cooperative hunting, mimics their crisscross pattern to optimize solutions. It maintains a population of feasible solutions, iteratively improving them over generations. CCHHO efficiently finds optimal 3DSDNN parameters by creating a evenly distributed population for maximized performance. The initial population of CCHHO is created randomwise using equation (15).

$$x_i = \begin{bmatrix} x_1^1 & x_2^1 & \dots & x_d^1 \\ x_1^2 & x_2^2 & \dots & x_d^2 \\ \vdots & \vdots & \dots & \vdots \\ x_1^N & x_2^N & \dots & x_d^N \end{bmatrix} \quad (15)$$

where x is total populace of seals whiskers in tracks; N is n^{th} number of CCHHO while attack to its prey, d is distance of prey and CCHHO. After initialization, the weight variable are generated randomly. Based on a conditional explicit hyper parameter scenario, the best fitness values are selected. It creates randomwise outcome from the initialized values. It is computed through optimizing parameter under equation (16).

$$\text{Fitness Function} = \text{optimizing } (h, d) \quad (16)$$

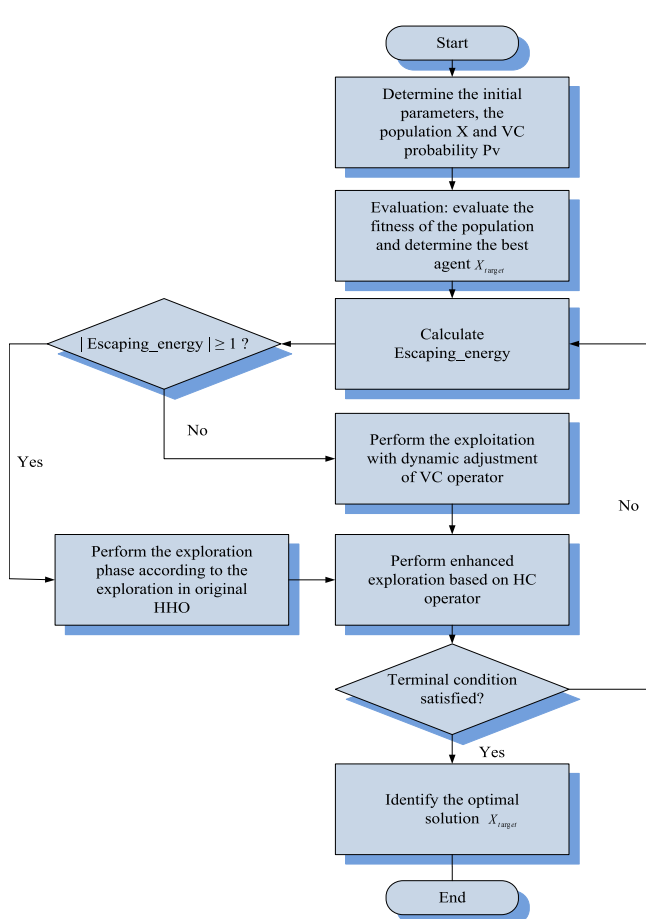


Fig. 3. Flowchart of CCHHO for optimizing 3DSDNN parameter.

here d represents the heterogeneous bi-directional DNN layer's output while dissimilar the image input, h denotes regression layer. When hunting, hawks employ four methods based on the prey's varying escape status. Four exploitative strategies based on the existing global optimum are developed to obtain search agents is enables the seal to determine the direction, vicinity and size of the prey using equation (17).

$$X_{average}(T) = \frac{1}{N} \sum_{i=1}^N X_i(T) \quad (17)$$

where ($X_{average}(T)$) is the majority of search agents currently work, ($X_i(T)$) reflects the search agent's (i^{th}) location at the time (T), ($X(T+1)$) and ($X(T)$) implies location of search agent in generation ($T + 1$) and (T). As an improved global search operator, enhanced exploration entails applying the HC search process to every search agent. Following the first two steps, this involved updating the entire population using equation (18).

$$Jump_{strength} = 2q \times (1 - r) \quad (18)$$

where (r) represents the location of an arbitrary agent and ($Jump_{strength}$) represent as the location of the best agent. Each generation generates (r) and (q) at random. Exploitation requires applying existing strategies to improve the current state of the optimization process. The ratio between exploration and exploitation is constantly changed during the optimization procedure, depends on the characteristics of the problem being solved. The individual for the final optimal calculation is given in equation (19).

$$\tilde{r} = \frac{\sum_{a=1}^M h^a W_{aj}^T}{\|d\|_\infty} \quad (19)$$

where d represents the heterogeneous bi-directional DNN layer's output while dissimilar the image input; h denotes regression layer; \tilde{r} represent as the row h^{th} and column d^{th} values of the output value matrix. The generator's weight value for variables h and d from 3D Shallow Deep Neural Network is optimized by CCHHO, otherwise it repeat iteratively step 3 until fulfill its halting conditions ($X = X + 1$). Then, 3DSDNN imperfectly assesses the quality of early classification and diagnosis of fruit diseases with increased accuracy and reduced computation time.

3.6. Hyperparameter selection

Initially, a range of learning rate from 1e to 4 to 1e-2 and batch sizes between 16 and 64 are explored using grid and random search strategies. The learning rate of 0.001 and batch size of 32 are selected as optimal under validation performance and computational constraints, balancing stable gradient updates with efficient memory usage. A count of epochs is set to 100 to allow sufficient training iterations while preventing overfitting, with early stopping employed for robustness. When the validation loss was flat, the adaptive learning rate scheduler reduced the learning rate by a factor of 0.001 to help fine-tune it during training. Regularization schemes like a dropout rate of 0.5 and weight decay are applied to improve generalization. The method utilized a 3×3 convolutional kernel with max pooling of size 2×2 , and the Crisscross Harris Hawks Optimizer facilitated effective weight updates. These combined strategies confirmed the stability and effectiveness of the chosen hyperparameters.

4. Result and discussion

The experimental outputs of EFDDNN-EI method have detected the strawberry diseases. Some performance analyses are conducted on parameters, such as computational time, f1-score, accuracy, recall and precision (Wu et al., 2024) and the outcomes are analyzed with existing

Table 2

Stimulation parameters of the proposed EFDDNN-EI.

Parameter	Value
Kernel Size (Convolution)	3×3
Pooling Type	Max Pooling
Pooling Size	2×2
Dropout	0.5
Learning Rate	0.001
Count of epoch	100
Batch size	32

SDD-TLDCNN (Karki et al., 2024), SDD-YOLOV5 (Chen et al., 2023) and SIFFD-DSGAN (Subha and Kasturi 2024) models respectively. **Table 2** presents the stimulation parameters of the EFDDNN-EI approach. **Figs. 4 and 5** portray the output results of strawberry and apple fruit disease datasets.

4.1. Experimental analysis

This section analyses the experimental evaluation of the proposed fruit disease classification approach. This section includes dataset and software requirements, training and validation description of experiment.

4.1.1. Training and validation of strawberry disease dataset

Fig. 6 depicts accuracy vs. epoch analysis. Here, 3DSDNN is trained with 9 classes. The accuracy of training reveals its presentation after the training demonstrated an impressive 99.72 % maximal training accuracy based upon a considerable training database consisting of

Strawberry disease images, inclusive of a 10 % overlap. In terms of validation, this figure shows higher accuracy of 99.82 % using the validation dataset again with equivalent over-lap. After that training, the method categorizes the input strawberry disease imageries accurately.

Fig. 7 specifies analysis of Loss over a count of epochs. The number of epochs indicates how many times the 3DSDNN will run on the entire training dataset. As the loss lowers, the number of epochs for the training and testing datasets increases. As epochs get better, the 3DSDNN exhibits a reduction in training and validation loss.

4.1.2. Training and validation of apple fruit disease dataset

Fig. 8 exposes accuracy vs. epoch of apple fruit disease dataset. The validation accuracy shows a gradual increase, stabilizing around 0.9 after approximately 40 epochs, while the method performs better on unseen data, it does not achieve perfect accuracy, likely due to overfitting or inherent complexity in the validation dataset. The validation accuracy fluctuates between 0.8 and 0.9 during the training, illustrating that while the model generalizes well, there is room for improvement in its ability to accurately predict validation samples as it approaches 100 epochs. The overall trend indicates a strong performance but highlights the importance of monitoring both training and validation metrics to ensure robust model performance.

Fig. 9 exemplifies the analysis of loss vs. epoch of apple fruit disease dataset. The training loss starts at 1.0 and declines steadily, signifying that the method is learning via the training data. The validation loss remains greater than the training loss, signifying potential overfitting as it plateaus around 0.4 while the training loss continues to decline towards 0.

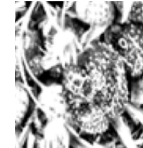
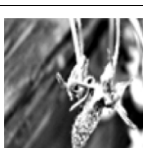
Input images	Pre-processed images	Classification	Input images	Pre-processed images	Classification
		Aphids			Slugs
		Healthy leaves			Sunburn
		Powdery mildew			Thrips
		Root rot			viral diseases
					vegetable green insects

Fig. 4. Output results of Strawberry Disease dataset.

Input images	Pre-processed images	Classification	Input images	Pre-processed images	Classification
		Blotch Apple			Normal Apple
		Rot Apple			Scab Apple

Fig. 5. Output results of Apple Fruit Disease dataset.

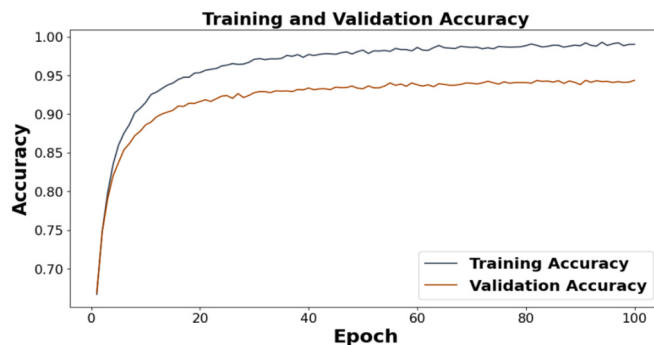


Fig. 6. Analysis of accuracy vs. epoch of Strawberry Disease dataset.

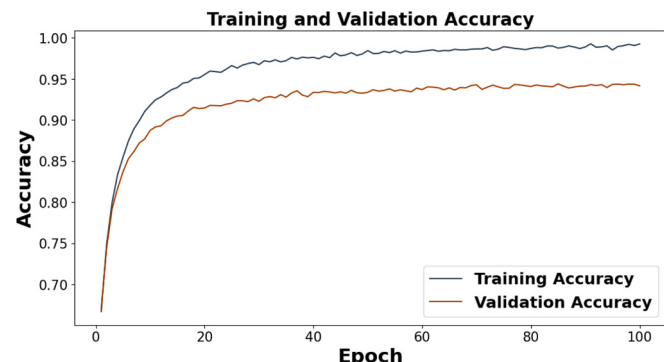


Fig. 8. Analysis of accuracy vs. epoch of Apple Fruit Disease dataset.

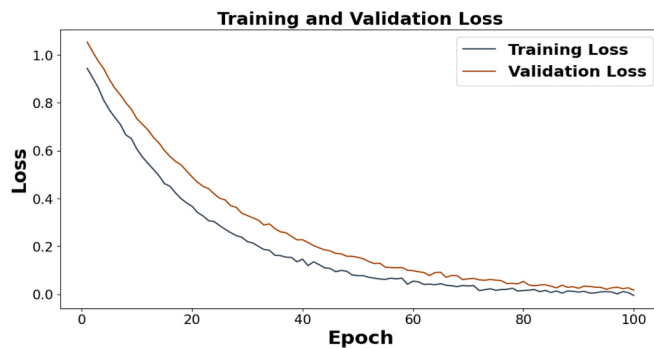


Fig. 7. Analysis of Loss vs. Epoch of Strawberry Disease dataset.

4.2. Performance analysis of strawberry disease dataset

Figs. 10 to 13 show the experimental outcomes of EFDDNN-EI method. Here, the performance of the EFDDNN-EI technique is evaluated with existing SDD-TLDCNN, SDD-YOLOV5 and SIFFD-DSGAN models.

Fig. 10 depicts the performance of testing accuracy analysis when the number of epochs increased, the classification testing accuracy increased as well. In this context, the proposed EFDDNN-EI method attains 19.56 %, 20.88 % and 29.60 % higher testing accuracy for powdery mildew; 16.10 %, 27.29 %, and 28.88 % higher testing accuracy for virus disease; 18.58 %, 27.87 % and 28.66 % higher testing accuracy for vegetables green insect; 12.16 %, 16.26 %, and 29.85 % higher testing accuracy for root rot; 19.56 %, 20.77 %, and 26.68 % higher testing accuracy for botrytis cinerea; 17.19 %, 18.26 %, and 28.89 % higher

testing accuracy for thrips; 17.59 %, 23.87 %, and 27.65 % higher testing accuracy for sunburn; 16.1 %, 35.2 % and 28.8 % higher testing accuracy for slug; 16.53 %, 22.84 % and 27.66 % higher testing accuracy for aphid and 19.56 %, 20.88 % and 29.60 % greater testing accuracy for healthy leaf over the existing SDD-TLDCNN, SDD-YOLOV5 and SIFFD-DSGAN respectively.

Fig. 11 shows recall analysis. The EFDDNN-EI method attains 19.58 %, 20.84 % and 29.46 % higher recall for powdery mildew; 16.17 %, 27.25 %, and 28.84 % higher recall for virus disease; 18.54 %, 27.84 % and 28.64 % higher recall for vegetables green insect; 12.41 %, 29.84 % and 36.82 % higher recall for root rot; 19.95 %, 20.67 % and 26.76 % higher recall for botrytis cinerea; 17.61 %, 28.48 % and 33.52 % higher recall for thrips; 17.65 %, 23.48 % and 27.26 % higher recall for sunburn; 16.31 %, 26.52 % and 28.28 % higher recall for slug; 16.35 %,

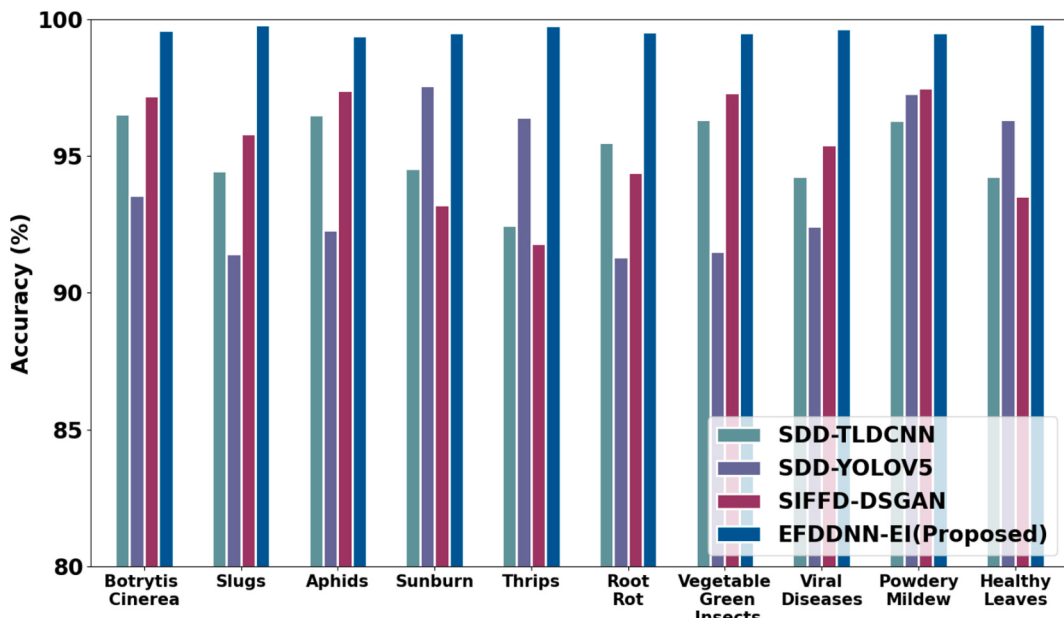


Fig. 10. Performance of Accuracy.

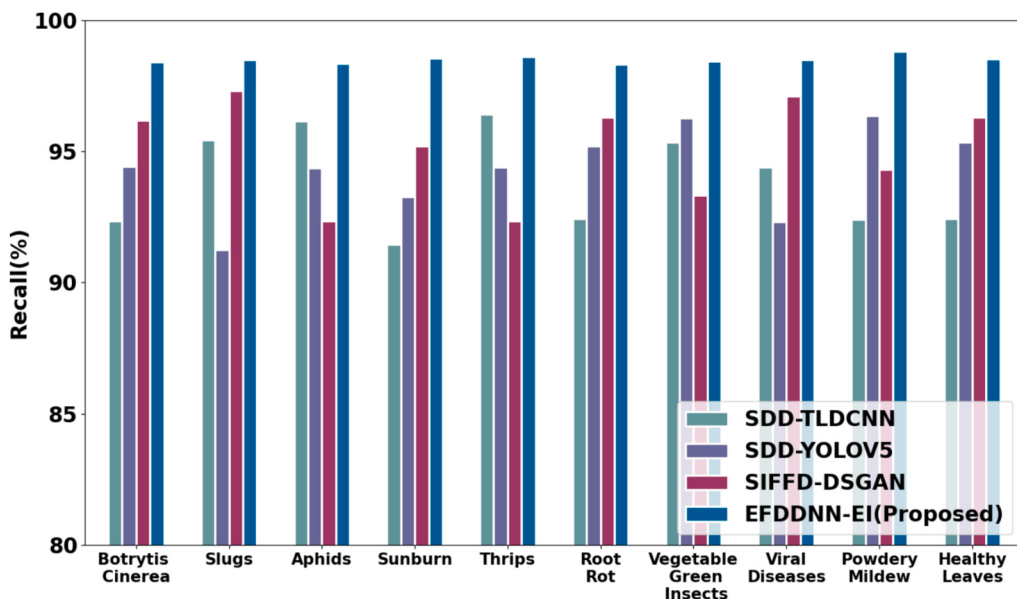


Fig. 11. Recall Analysis.

22.38 % and 27.46 % higher recall for aphid and 19.58 %, 20.84 % and 29.46 % higher recall for healthy leaf compared to the existing SDD-TLDCNN, SDD-YOLOV5 and SDD-LCDL-CS models.

Fig. 12 shows precision analysis. Precision is frequently taken into account in conjunction with other measures to offer a complete data. In this context, the EFDDNN-EI technique achieves 19.53 %, 20.85 %, and 29.66 % higher precision for Powdery mildew; 16.12 %, 28.84 % and 37.25 %, higher precision for virus disease; 18.56 %, 27.84 % and 28.67 % higher precision for vegetables green insect; 12.19 %, 27.23 % and 29.85 % higher precision for root rot; 19.54 %, 20.76 % and 26.65 % higher precision for botrytis cinerea; 17.15 %, 28.87 % and 31.26 % higher precision for thrips; 17.45 %, 23.58 % and 27.76 % higher precision for sunburn; 16.61 %, 29.52 % and 28.38 % higher precision for slug; 16.45 %, 27.36 % and 27.58 % higher precision for aphid and

19.53 %, 20.85 % and 29.66 % higher precision for healthy leaf over the existing SDD-TLDCNN, SDD-YOLOV5 and SIFFD-DSGAN.

Fig. 13 depicts f1-score analysis. The EFDDNN-EI method attains 19.83 %, 21.57 % and 29.65 % higher f1-score for powdery mildew; 16.14 %, 27.27 % and 28.78 % higher f1-score for virus disease; 16.78 %, 18.65 % and 22.56 % higher f1-score for vegetables green insect; 12.14 %, 16.25 % and 29.48 % higher f1-score for root rot; 19.56 %, 20.77 % and 26.64 % higher f1-score for botrytis cinerea; 17.14 %, 21.26 % and 27.87 % high f1-score for thrips; 20.78 %, 23.87 % and 27.66 % high f1-score for sunburn; 16.17 %, 24.22 % and 28.84 % higher f1-score for slug; 16.58 %, 27.88 % and 27.68 % higher f1-score for aphid and 19.83 %, 21.57 % and 29.65 % high f1-score for healthy leaf evaluated with existing SDD-TLDCNN, SDD-YOLOV5 and SIFFD-DSGAN respectively.

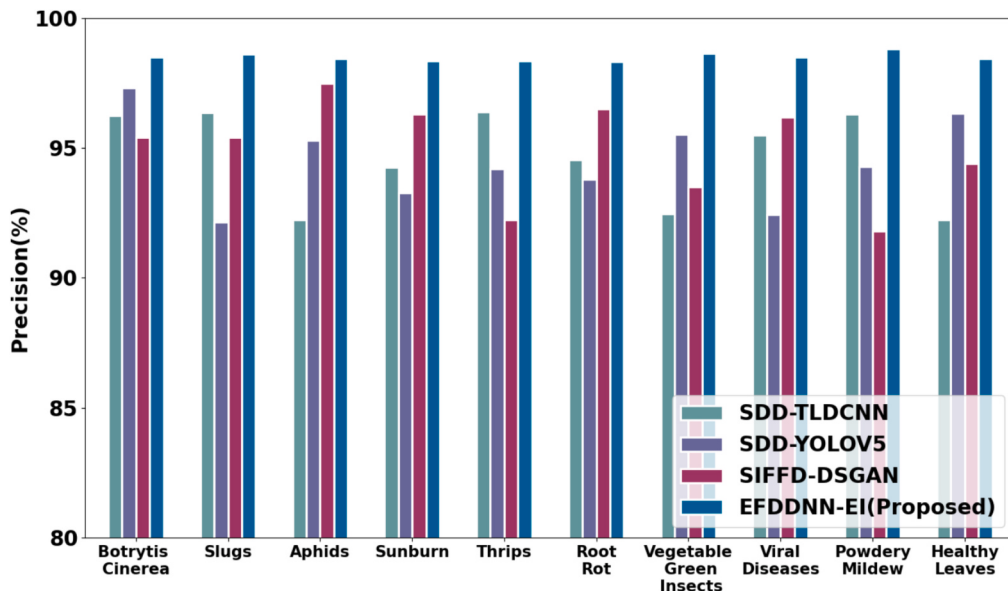


Fig. 12. Performance of Precision.

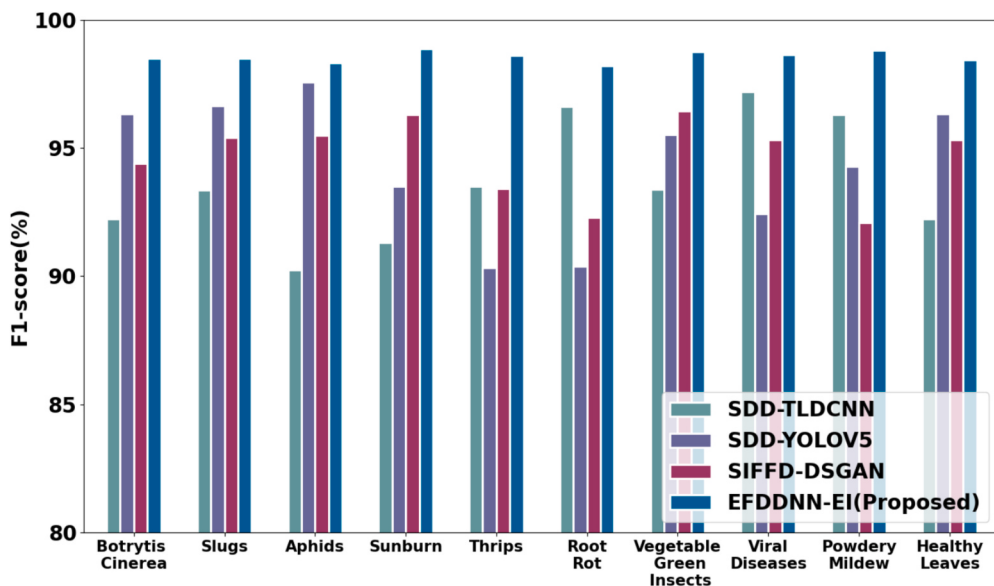


Fig. 13. F1-score evaluation.

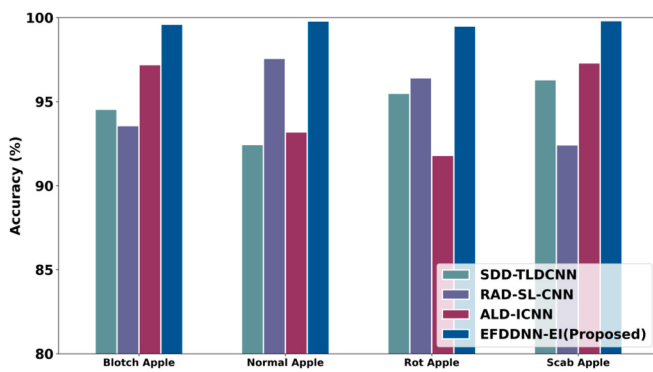


Fig. 14. Performance of Accuracy.

4.3. Performance analysis of apple fruit disease dataset

Figs. 14 to 20 portray the simulation results of EFDDNN-EI method. Here, the performance of proposed EFDDNN-EI is analysed with other SDD-TLDCNN (Subha and Kasturi 2024), RAD-SL-CNN (Paliwal et al., 2024) and ALD-ICNN (Acharya and Ravi 2024) approaches.

Fig. 14 expresses accuracy analysis. CCHHO enhances accuracy by integrating evolutionary strategies and dynamic scaling factors, which improve exploration in initial search phases and exploitation in later stages. The proposed EDCP-O3DSDNN-XCTIN attains 20.28 %, 18.22 % and 19.27 % higher accuracy for normal apple; 26.29 %, 17.31 %, and 17.26 % higher accuracy for blotch apple; 24.28 %, 13.22 % and 19.27 % higher accuracy for rot apple; 27.28 %, 18.22 % and 12.27 % higher accuracy for scab apple than the existing SDD-TLDCNN, RAD-SL-CNN and ALD-ICNN methods.

Fig. 15 indicates the proposed model Sensitivity analysis. The 3DSDNN enhances sensitivity by effectively prioritizing relevant temporal features through attention mechanisms, allowing it to focus on fruit disease classification. The proposed EFDDNN-EI attains 13.26 %, 19.22 %, and 17.27 % higher recall for normal apple; 18.26 %, 13.69 %, and 16.35 % higher recall for blotch apple; 18.26 %, 15.69 %, and 16.35 % higher recall for rot apple; 15.26 %, 13.19 %, and 16.35 % higher recall for scab apple comparing to the existing as SDD-TLDCNN, RAD-SL-CNN and ALD-ICNN models.

Fig. 16 represents precision analysis. In which, 3DSDNN enhances precision in fruit disease classification by effectively focusing on relevant temporal features and relationships within the data. By utilizing attention mechanisms, 3DSDNN prioritizes critical information, allowing for more precise categorization of covid-19 disease. The EFDDNN-EI attains 13.26 %, 19.22 %, and 17.27 % higher precision for normal

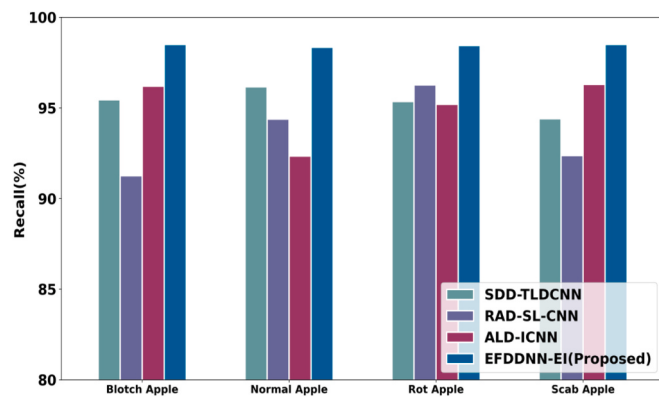


Fig. 15. Performance of Recall.

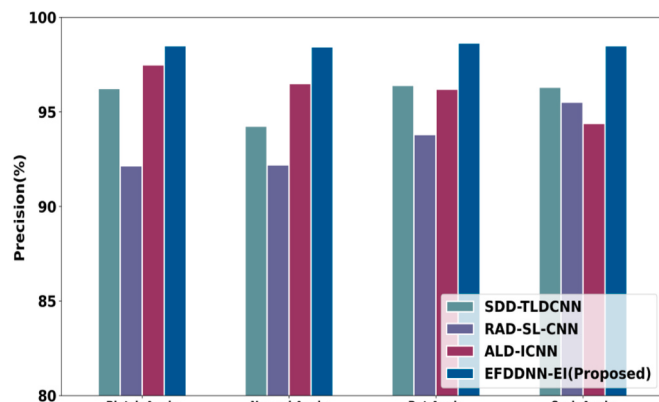


Fig. 16. Analysis of Precision.

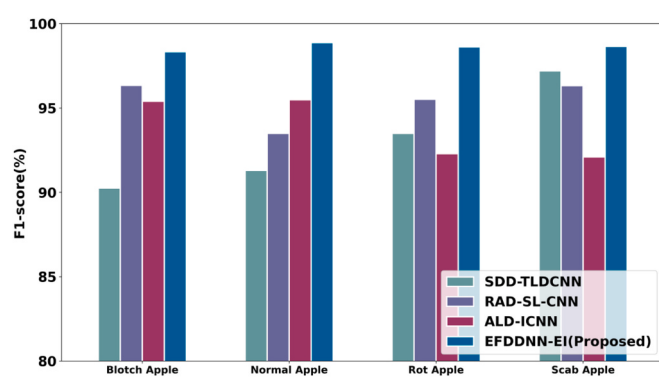


Fig. 17. Analysis of F1-score.

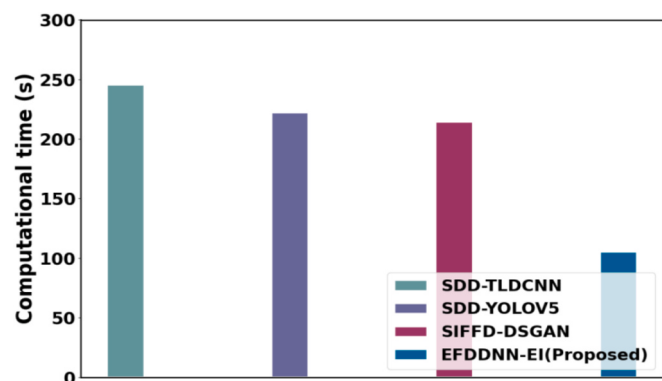


Fig. 18. Analysis of Computational Time.

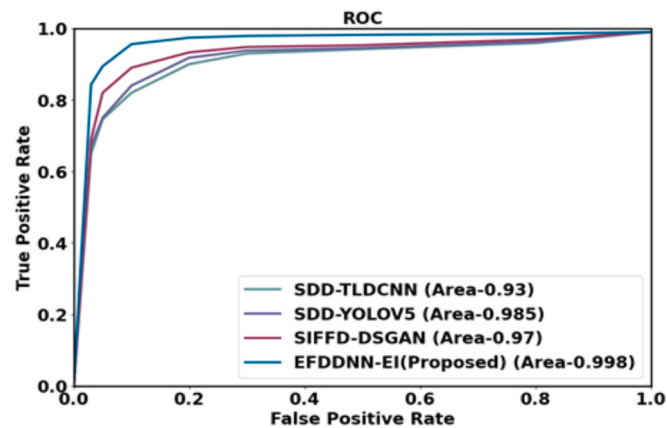


Fig. 19. ROC analysis.

apple; 18.26 %, 13.69 %, and 16.35 % higher precision for blotch apple; 15.26 %, 16.69 %, and 18.35 % higher precision for rot apple; 18.26 %, 13.69 %, and 16.35 % higher precision for scab apple compared to the existing SDD-TLDCNN, RAD-SL-CNN and ALD-ICNN methods.

The f1-score analysis is depicted in **Fig. 17**. In this, 3DSDNN enhances precision in fruit disease classification by effectively integrating temporal attention mechanisms that prioritize relevant features over time, coupled with graph convolutional networks that capture complex spatial relationships, thereby increasing the model's capacity to discern subtle disease cues in fruits. The proposed EFDDNN-EI attains 18.26 %, 15.22 %, and 12.27 % higher f1-score for normal apple; 15.26 %, 10.59 %, and 16.35 % greater f1-score for blotch apple; 15.26 %, 10.59 % and 18.35 % greater f1-score for rot apple; 15.26 %, 10.59 % and 16.35 % greater f1-score for scab apple than the existing SDD-TLDCNN, RAD-SL-CNN and ALD-ICNN model.

Fig. 18 exhibits computation time assesment, the comparison of the efficacy of the proposed fruit disease classification based on an optimized 3DSDNN. Here, the EFDDNN-EI technique achieves 18.84 %, 20.53 %, and 24.66 % reduced computing time when compared to the existing SDD-TLDCNN, SDD-YOLOV5 and SIFFD-DSGAN models respectively.

Fig. 19 shows ROC analysis. Here, True Positive Rate (sensitivity) is plotted against False Positive Rate. Area under the ROC curve indicates the overall effectiveness of each model. Among the models, EFDDNN-EI achieves the greater AUC of 0.998, demonstrating near-perfect classification capability. It significantly outperforms SDD-TLDCNN (AUC: 0.93), SIFFD-DSGAN (AUC: 0.97), and SDD-YOLOV5 (AUC: 0.985). These results confirm the proposed EFDDNN-EI model's superior predictive accuracy and reliability in minimizing false positives while maximizing true detections.

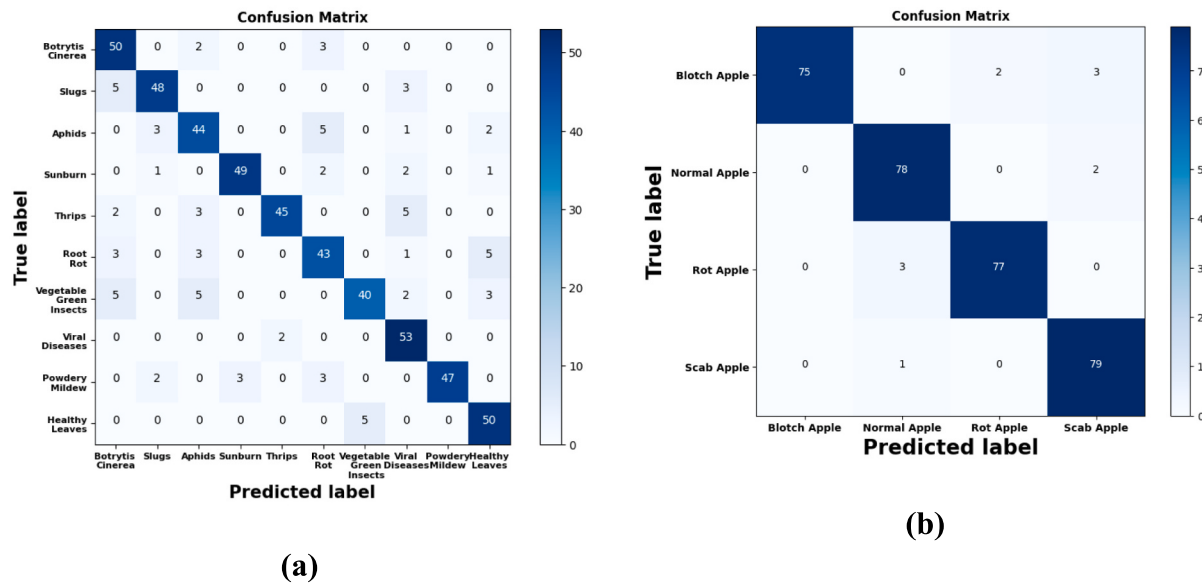


Fig. 20. Confusion Matrix of (a) strawberry diseases dataset and (b) apple fruit disease dataset.

Fig. 20 depicts the combined confusion matrix for strawberry diseases dataset (a) and the apple fruit disease dataset (b). The figure compares the two confusion matrices in images (a) and (b), showing that both datasets perform equally in terms of classification. The first matrix evaluates a model trained to detect four apple conditions: blotch, normal, rot, scab. It achieves better results with 75 correct predictions for blotch apple, 78 for normal apple, 77 for rot apple, 79 for scab apple, demonstrating high overall accuracy. Misclassifications are minimal: blotch apples are confused three times as scab apples and twice as rot apples; normal apples are misclassified only twice as scab apples; rot apples are confused three times as normal apples; and scab apples are mislabeled once as a normal apple. The second matrix presents classification results across ten plant health categories, including both diseased and healthy leaves with each class containing 50 samples. Most diagonal values are high, indicating better classification rates for classes like botrytis cinerea (50), sunburn (49) and viral diseases (53). Misclassifications are relatively few but noticeable in certain categories. For example, Vegetable green insects were often confused with botrytis cinerea and aphids, while root rot was occasionally mistaken for healthy leaves. Overall, both classifiers demonstrate reliable performance with only minor confusion occurring between visually or symptomatically similar classes.

Table 3 displays performance comparison of various model configurations reveals the impact of each component on accuracy, precision, recall, f1-score and computational efficiency. The EFDDNN-EI achieves better accuracy 99.37 %, precision 98.56 %, recall 98.89 %, f1-score 98.72 % with less computational time 21.9 s, indicating superior performance and efficiency. Removing the CCHHO component results in a noticeable drop in all metrics, with accuracy decreasing to 90.75 % and computational time increasing to 52.7 s. Further exclusion of the NTEWT component shows a continued decline in performance, while also increasing the processing time to 48.5 s. The model without only the

RBAEKF component maintains a relatively high accuracy of 96.4 % but with slightly reduced precision and recall, and a computational time of 38.2 s. These results highlight the significance of each component, particularly the contribution of CCHHO and NTEWT to both performance accuracy and efficiency.

Table 4 presents a performance comparison of image denoising methods. Among all methods, RBAEKF demonstrates the highest performance, achieving an accuracy of 99.37 % and a precision of 98.56 %, which indicates its effectiveness in enhancing the clarity of input images for classification. Additionally, it records the highest PSNR of 31.89 dB, reflecting superior noise suppression capability, and the highest SSIM of 0.911, signifying better structural preservation of image content. In contrast, traditional methods like GF, MF, and BF show lower accuracy (ranging from 91.34 % to 92.76 %) and lower PSNR and SSIM values, indicating less effective noise reduction and feature retention. These outcomes show the significant advantages of RBAEKF in improving both image quality and the downstream classification performance in fruit disease detection.

Table 4
Performance comparison of image denoising Methods.

Methods	Accuracy (%)	Precision (%)	PSNR (dB)	SSIM
Gaussian Filter (GF) (Fischer-Brandies et al., 2025)	91.34	89.26	25.71	0.779
Median Filter (MF) (Zhang et al., 2023)	92.11	90.14	27.56	0.812
Bilateral Filter (BF) (Abuhayi and Bezabh, 2023)	92.76	90.72	28.24	0.834
RBAEKF (Proposed)	99.37	98.56	31.89	0.911

Table 3
Ablation study of EFDDNN-EI.

Component	Computational Time (s)	F1-Score (%)	Accuracy (%)	Recall (%)	Precision (%)
Without RBAEKF	38.2	92.79	96.4	92.5	93.1
Without RBAEKF + NTEWT	48.5	91.62	91.6	91.8	91.45
Without RBAEKF + NTEWT + without CCHHO	52.7	90.1	90.75	90.1	90.1
EFDDNN-EI (with full model)	21.9	98.72	99.37	98.89	98.56

4.4. Discussion

This paper proposes an EFDDNN-EI model for detecting strawberry leaf diseases using a mentioned image datasets. The method involves RBAEKF-based preprocessing, NTEWT feature extraction and 3DSDDNN classification enhanced by the CCHHO optimization technique to reduce overfitting. It accurately classifies the diseases, such as botrytis cinerea, aphids, thrips, sunburn, root rot, viral infections. EFDDNN-EI achieves 96.94 % precision, outperforming existing SDD-TLDCNN, YOLOv5 and SIFFD-DSGAN approaches in both accuracy and efficiency. The model also offers less computational cost, making it reliable and cost-effective solution in agriculture for real-time disease detection.

5. Conclusion

In this work, Strawberry Diseases Detection Using 3D Shallow Deep Neural Network and Crisscross Harris Hawks Optimizer (EFDDNN-EI) was implemented successfully. The EFDDNN-EI was used to detected strawberry diseases exactly. The outcomes highlight distinct enhancements and attained 19.53 %, 20.85 % and 29.66 % higher precision, 19.83 %, 21.57 % and 29.65 % higher f1-score, 18.84 %, 20.53 % and 24.66 % lower computational time compared to the existing SDD-TLDCNN, SDD-YOLOV5 and SIFFD-DSGAN models respectively. It intends to use the most recent high-performance benchmark model and optimize the network architecture in future studies to increase the detection performance. To make the model more user-friendly and accessible for farmers and it intend to implement it for the use of integrated mobile devices in real-time strawberry disease identification in greenhouses.

CRediT authorship contribution statement

Hridaynath Pandurang Khandagale: Conceptualization, Methodology, Writing – original draft. **Sangram Tukaram Patil:** Supervision. **Vikram Sampat Gavali:** Supervision. **Amrita Arvind Manjrekar:** Supervision. **Pratap Pandurang Halkarnikar:** Supervision.

Declaration of competing interest

The authors declare that they have no known competing financial interests or personal relationships that could have appeared to influence the work reported in this paper.

Data availability

No data was used for the research described in the article.

References

- Abuhayi, B. M., & Bezabih, Y. A. (2023). Chickpea disease classification using hybrid method. *Smart Agric. Technol.*, 6, Article 100371.
- Acharya, V., & Ravi, V. (2024). Apple foliar leaf disease detection through improved capsule neural network architecture. *Multimed. Tools Appl.*, 83(16), 48585–48605.
- Ahmed, I., & Yadav, P. K. (2024). Predicting apple plant diseases in orchards using machine learning and deep learning algorithms. *SN Comput. Sci.*, 5(6), 700.
- Annapoorna, B. R. (2024). Enhancing Breast Cancer Detection With Ensemble Methods: A Comprehensive Analysis. *Journal of Electrical Systems*, 20(10), 5118–5132.
- Azizi, H., Asli-Ardeh, E. A., Jahanbakhshi, A., & Momeny, M. (2024). Vision-based strawberry classification using generalized and robust deep networks. *Journal of Agriculture and Food Research*, 15, Article 100931.
- Chen, S., Liao, Y., Lin, F., & Huang, B. (2023). An Improved Lightweight Yolov5 Algorithm For Detecting Strawberry Diseases. Ieee Access.
- Balu, S., Ganapathy, D., Arya, S., Atchudan, R., & Sundaramoorthy, A. K. (2024). Advanced photocatalytic materials based degradation of micropollutants and their use in hydrogen production—a review. *RSC advances*, 14(20), 14392–14424.
- Crespo, A., Moncada, C., Crespo, F., & Morochó-Cayamcela, M. E. (2025). An efficient strawberry segmentation model based on Mask R-CNN and TensorRT. *Artif. Intell. Agric.*
- Fischer-Brandies, L., Müller, L., Rieger, J.J. & Buettner, R., (2025). Fresh or Rotten? Enhancing Rotten Fruit Detection With Deep Learning and Gaussian Filtering. *IEEE Access*.
- Fischer-Brandies, L., Müller, L., Rieger, J.J. & Buettner, R., (2025). Fresh or Rotten? Enhancing Rotten Fruit Detection With Deep Learning and Gaussian Filtering. *IEEE Access*.
- Guo, Z., Zhang, Y., Xiao, H., Jayan, H., Majeed, U., Ashigbor, K., Jiang, S., & Zou, X. (2025). Multi-sensor fusion and deep learning for batch monitoring and real-time warning of apple spoilage. *Food Control*, Article 111174.
- Gupta, S., & Tripathi, A. K. (2024). Fruit and vegetable disease detection and classification: recent trends, challenges, and future opportunities. *Eng. Appl. Artif. Intel.*, 133, Article 108260.
- Gupta, S., Tripathi, A. K., & Lewis, N. (2025). Pre-trained noise based unsupervised GAN for fruit disease classification in imbalanced datasets. *Pattern Anal. Appl.*, 28(2), 39.
- Haq, I. U., Kaur, G., & Rather, A. H. (2024). Fruit leaf classification using transfer learning for automation and industrial applications. *Deep Learning Techniques for Automation and Industrial Applications*, 151–178.
- <https://universe.roboflow.com/research-proj/strawberry-diseases-detection/dataset/1>.
<https://www.kaggle.com/datasets/anilsandhii/apple-fruit-disease-images-dataset>.
- Hu, D., Qiu, D., Yu, S., Jia, T., Zhou, T., & Yan, X. (2024). Integration of optical property mapping and machine learning for real-time classification of early bruises of apples. *Food Bioproc. Tech.*, 17(9), 2745–2756.
- Iqbal, M., Haider, S. T., Shoukat, R. S., Rehman, S. U., Mahmood, K., Villar, S. G., Lopez, L. A. D., & Ashraf, I. (2025). Canned apple fruit freshness detection using hybrid convolutional neural network and transfer learning. *J. Food Qual.*, 2025(1), Article 8522400.
- Jeong, H., Moon, H., Jeong, Y., Kwon, H., Kim, C., Lee, Y., Yang, S., & Kim, S. (2024). Automated technology for strawberry size measurement and weight prediction using AI. *IEEE Access*, 12, 14157–14167.
- Karki, S., Basak, J. K., Tamrakar, N., Deb, N. C., Paudel, B., Kook, J. H., Kang, M. Y., Kang, D. Y., & Kim, H. T. (2024). Strawberry disease detection using transfer learning of deep convolutional neural networks. *Scientia Horticulturae*, 332, Article 113241.
- Kausar, A., Razzak, I., Shapiai, M. I., & Beheshti, A. (2023). 3D shallow deep neural network for fast and precise segmentation of left atrium. *Multimedia Syst.*, 29(3), 1739–1749.
- Li, W., Auger, F., Zhang, Z., & Zhu, X. (2023). Newton time-extracting wavelet transform: an effective tool for characterizing frequency-varying signals with weakly-separated components and theoretical analysis. *Signal Process.*, 209, Article 109017.
- Liu, S., Ampatzidis, Y., Zhou, C., & Lee, W. S. (2025). AI-driven time series analysis for predicting strawberry weekly yields integrating fruit monitoring and weather data for optimized harvest planning. *Comput. Electron. Agric.*, 233, Article 110212.
- Mehta, S., Singh, G., & Bhale, Y. A. (2024). Precision Agriculture: An Augmented Datasets and CNN Model-Based Approach to Diagnose Diseases in Fruits and Vegetable Crops. *Simulation Techniques of Digital Twin in Real-Time Applications: Design Modeling and Implementation*, pp. 215–242.
- Nguyen, D. K., Choi, Y. S., Lee, J. H., Tran, M. T., & Xin, X. (2024). An effective deep learning model for classifying diseases on strawberry leaves and estimating their severity based on the multi-task U-Net. *Multimed. Tools Appl.*, 1–22.
- Nóvoa, A., Racca, A., & Magri, L. (2024). Inferring unknown unknowns: regularized bias-aware ensemble Kalman filter. *Comput. Methods Appl. Mech. Eng.*, 418, Article 116502.
- Oliullah, K., Islam, M. R., Babar, J. I., Quraishi, M. N., Rahman, M. M., Mahbub-Or-Rashid, M., & Bhuiyan, T. A. U. H. (2025). FruVeg MultiNet: a hybrid deep learning-enabled IoT system for fresh fruit and vegetable identification with web interface and customized blind glasses for visually impaired individuals. *Journal of Agriculture and Food Research*, 19, Article 101623.
- Paliwal, M., Singh, G., Soni, P., & Kaur, R., (2024). Rotten Apple Detection System Based on Deep Learning using Convolution Neural Network. In *Computational Intelligence and Mathematical Applications* (pp. 161–167). CRC Press.
- Raza, S. M., Raza, A., Babiker, M. I. A., Haq, Z. U., Islam, M. A., & Li, S. (2024). Improving citrus fruit classification with x-ray images using features enhanced vision transformer architecture. *Food Anal. Methods*, 17(11), 1523–1539.
- Selvaraj, K., Venkatesan, L. S., Ganapathy, D., & Sathishkumar, P. (2024). Treatment of dental biofilm-forming bacterium Streptococcus mutans using tannic acid-mediated gold nanoparticles. *Microbial pathogenesis*, 189, 106568.
- Shafik, W., Tufail, A., De Silva Liyanage, C., & Apong, R. A. A. H. M. (2024). Using transfer learning-based plant disease classification and detection for sustainable agriculture. *BMC Plant Biol.*, 24(1), 136.
- Subha, V., & Kasturi, K. (2024). Structural invariant feature segmentation based apple fruit disease detection using deep spectral generative adversarial networks. *SN Comput. Sci.*, 5(5), 635.
- Upadhyay, N., & Gupta, N. (2024). Diagnosis of fungi affected apple crop disease using improved ResNeXt deep learning model. *Multimed. Tools Appl.*, 83(24), 64879–64898.
- Wang, W., Zhu, A., Wei, H., & Yu, L. (2024). A novel method for vegetable and fruit classification based on using diffusion maps and machine learning. *Curr. Res. Food Sci.*, 8, Article 100737.

- Wang, X., Dong, X., Zhang, Y., & Chen, H. (2023). Crisscross harris hawks optimizer for global tasks and feature selection. *J. Bionic Eng.*, 20(3), 1153–1174.
- Wu, G., Fang, Y., Jiang, Q., Cui, M., Li, N., Ou, Y., Diao, Z., & Zhang, B. (2023). Early identification of strawberry leaves disease utilizing hyperspectral imaging combining with spectral features, multiple vegetation indices and textural features. *Comput. Electron. Agric.*, 204, Article 107553.
- Wu, J., Abolghasemi, V., Anisi, M. H., Dar, U., Ivanov, A., & Newenham, C. (2024). Strawberry disease detection through an advanced squeeze-and-excitation deep learning model. *IEEE Transactions on AgriFood Electronics*.
- Zhang, B., Ou, Y., Yu, S., Liu, Y., Liu, Y., & Qiu, W. (2023). Gray mold and anthracnose disease detection on strawberry leaves using hyperspectral imaging. *Plant Methods*, 19(1), 148.
- Zhang, T., Guan, H., Ma, X., & Shen, P. (2023). Drought recognition based on feature extraction of multispectral images for the soybean canopy. *Eco. Inform.*, 77, Article 102248.